DNS STUDY ON THE MEASUREMENT OF TURBULENT WALL SHEAR STRESS USING SURFACE-MOUNTED HOT-FILM SENSOR

Takeshi Kouno, Shinnosuke Obi, and Shigeaki Masuda
Department of Mechanical Engineering, Keio University
3-14-1 Hiyoshi, Kohoku-ku, 223-8522 Yokohama, Japan
obsn@mech.keio.ac.jp (S. Obi)

ABSTRACT

The influence of heat conduction on the response of a surface-mounted hot-film sensor has been numerically investigated with special attention paid to turbulent wall shear stress measurements. Energy transport equation is solved for both fluid and solid parts, where the thermal conductivity of the solid part is varied to realize various materials common in constructing the wind tunnel wall, and a sensor operating under the constant temperature is emulated. The results indicate that the better signal is obtained by the sensor when it is attached on the wall whose thermal conductivity is higher than that of the substrate. It is the heat flow from the hot-film transferred in the substrate by conduction, that contaminates the response of the sensor, because the enlargement of the virtual size of the sensor due to conduction results in low streamwise resolution.

INTRODUCTION

The flush-mounted hot-film sensor is common in measuring wall shear stress in wall-attached boundary layer flows. The heat transferred to the fluid by convection, Q, and the wall shear stress τ_w are correlated by:

$$Q = A\tau_w^{1/3} + B, \qquad (1)$$

where A and B are empirical constants. The constants A and B are usually calibrated in steady condition, and the same values are used for measurements in unsteady flows.

It is a common belief that the heat conduction into solid wall is the major error source in the measurement of turbulent wall shear stress using a hot-film sensor, particularly for the measurements in the air. To minimize this effect, the insulation of the hot-film sensor from the wall has been a common practice, by, e.g., setting a cavity behind the sensor (Alfredsson et al., 1988). However, when the higher order turbulence statistics are concerned, some experiments indicate that the effect appears in rather opposite manner, i.e., wall materials with higher heat conduction provide a better result than that with lower heat conduction (Dengel et al., 1987). The explanation on the associating physics is necessary, when the increasing interest to the application of micro sensor technology to flow control is considered because the wall-attached hot-film sensor is used to detect instantaneous wall shear stress variation (e.g., Kimura et al., 1999).

The influence of the heat conduction to the solid wall has been investigated both experimentally and numerically. Reda (1991) studied the influence of the thermal property of the hot-film substrate, and suggested that the effective thermal length of the sensor is the important factor for quick response of the sensor. Moen and Schneider (1993) performed an experimental study on the effect of heat conduction in the substrate of hot-film sensor. They have shown the region of high temperature around the sensor is enlarged when the thermal impedance of substrate is high, though the details of its influence on the output signal of the sensor are left unexplored. In an later publication (Moen and Schneider, 1994), they have mentioned the advantage of a small sensor over larger ones in terms of the better frequency response. The numerical study by Tardu et al. (1991) supports essentially the same fact that the longitudinal thermal diffusion contaminates the output of the hot-film. The experiments by Cock (1994), where the sensor that is not glued on a substrate but kept in a cavity has better characteristics than the sensor with substrate, strongly suggests that the bad frequency response of a flush-mounted hot-film sensor is not solely determined by the material of the wall, but the thermal property of the substrate must be taken into account.

To obtain the detailed information for the above-mentioned situation, the direct numerical simulations (DNS) for turbulent channel flow are performed in the present study. The thermal field around the hot-film sensor is computed for various wall materials, with the existence of the substrate taken into account. The relationship between the fluid motion responsible for the fluctuating wall shear stress and the output of the hot-film is clarified by analyzing the heat flux from the sensor.

COMPUTATION

Fully Developed Turbulent Channel Flow

Prior to the computation of thermal field, DNS of a fully developed turbulent channel flow was performed at $Re = 150$, with Re being the Reynolds number based on the friction velocity and half the channel width. The dimension of the whole computation domain was $L_x^+ \times L_y^+ \times L_z^+ = 1152 \times 300 \times 576$, with L_x^+, L_y^+, L_z^+ being the length in the streamwise direction (x), wall-normal direction (y), and the spanwise direction (z), all normalized by the wall unit. 64 numerical grids covered each direction; resulting grid resolution in the x- and z-directions was 18.0 and 9.0, respectively. The periodic boundary condition was applied at the inlet and outlet planes to achieve the fully developed turbulent channel flow. The numerical method was based on the fourth-order central differencing scheme developed by Kajishima et al. (1998). The entire domain for the fluid flow computation is shown in Fig. 1, where the calculated instantaneous wall shear stress distribution is illustrated.

Computation of the Thermal Field

Regarding the fluid temperature to be a passive scalar, the transport equation for temperature was solved:

$$\frac{\partial T}{\partial t} + \mathrm{div}(\vec{v}T) = \frac{k}{\rho c_P}\mathrm{div}(\mathrm{grad}\, T). \quad (2)$$

The computation was performed for both the fluid part and the solid wall part. In the fluid part, the velocity components in three directions, appearing in the convection terms, were supplied by the DNS that was performed separately. The temperature distribution in the solid wall part was determined solely by the heat conduction.

Due to the small size of the hot-film sensor compared to the grid size used for the channel flow DNS, cf. Fig. 1, it was impossible to solve the velocity and temperature simultaneously. Instead, the computation of thermal field was performed for the smaller region covering both the fluid and the solid wall part surrounding the hot-film sensor as shown in Fig. 2. The thermal computation domain extended $l_x^+ \times l_y^+ \times l_z^+ = 45 \times 23.4 \times 90$. The number of grids covering this region was $50 \times 52 \times 50$, uniform in all directions.

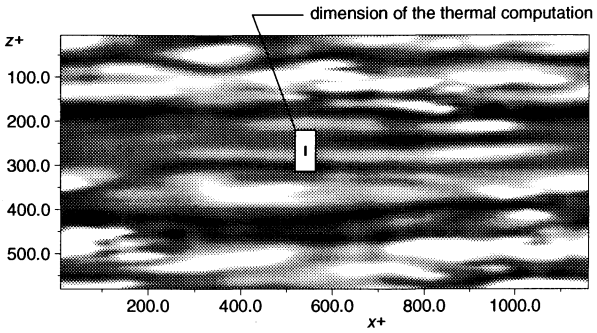

Figure 1: Entire computation domain for fluid flow. The hot-film sensor is marked on the center of the thermal computation domain.

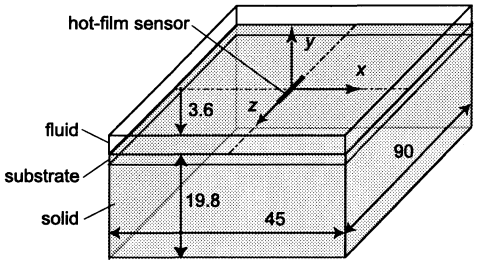

Figure 2: Computation domain for thermal field around the hot-film sensor. Numbers are in wall unit.

The sensor was represented by two rows of computational grids along which the constant temperature was specified to emulate a constant temperature anemometer. The dimension of the sensor was determined, by referring a commercial sensor (DANTEC 55R47), to be 1.8 and 18 in wall unit in the streamwise and spanwise directions, respectively. It is supposed that the hot-film sensor deposits on a 1.8 wall-unit thick polymide substrate that is further glued on the wall of object whose wall shear stress is to be measured. The thickness of the sensor itself, the coating film of quartz above it, and the glue lamina were not taken into account because of the negligible thickness as compared to that of the polymide substrate.

Computations were performed for selected wall materials summarized in Table 1. The case in which a cavity is set beneath the hot-film in attempt to isolate the sensor from the wall was emulated by setting the wall properties equal to that of the air. The temperature of the oncoming air was set equal to 20°C,

Table 1: Properties of wall materials.

Material	k W/mK	$\rho \times 10^3$ kg/m^3	$c_P \times 10^3$ J/kgK
Polymide	0.42	1.47	1.17
Air	0.0257	0.00117	1.005
Acrylic	0.20	1.10	1.85
Quartz Glass	1.5	2.22	0.84
Steel	80.3	7.87	0.442
Aluminum	203	2.70	0.90

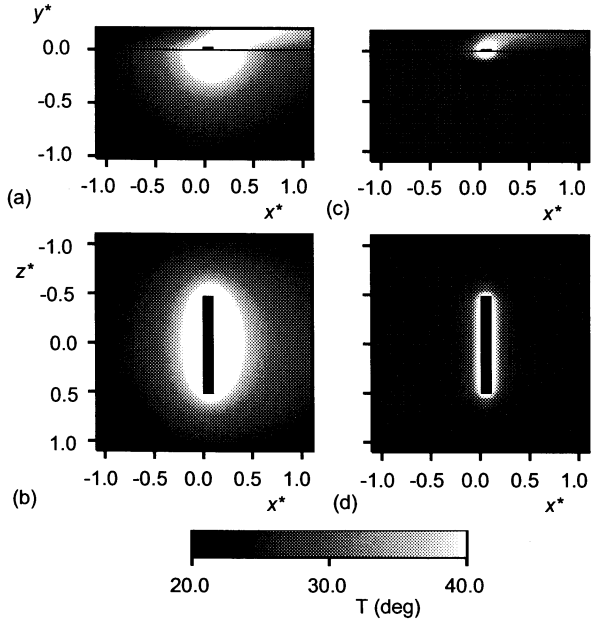

Figure 3: Temperature distribution around the hot-film sensor. (a), (b) Acrylic wall, (c), (d) aluminum.

while the sensor temperature was set constant to 80°C. Neumann condition was applied at the boundary of the thermal computation domain. For the calculation of turbulence statistics, a slight increase in the temperature in the solid part due to the accumulation of energy was corrected by approximating the temperature increase by linear polynomial.

Calculation of the Hot-Film Output

The output signal from the hot-film sensor was evaluated by the sum of the heat flux to the fluid flow Q_F and the heat flux to the wall through substrate, Q_S. They were calculated by:

$$Q_F = -k_F \iint \left.\frac{\partial T}{\partial y}\right|_{y=+0} dx\, dz, \quad (3)$$

$$Q_S = -k_S \iint \left.\frac{\partial T}{\partial y}\right|_{y=-0} dx\, dz, \quad (4)$$

with k_F and k_S being the thermal conductivity of the fluid and substrate, respectively. The surface integration was performed over the entire area of the hot-film sensor. The sum of

Table 2: Turbulence statistics for various wall materials.

Wall	τ_w'	SF (dynamic)
Cavity	0.05	0.05 (-0.027)
Acrylic	0.10	0.11 (0.52)
Quartz Glass	0.16	0.26 (0.58)
Steel	0.21	0.40 (0.65)
Aluminum	0.20	0.34 (0.80)
true value	0.36	0.95

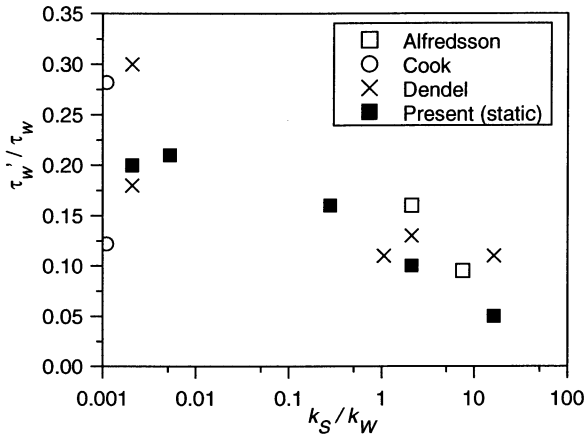

Figure 4: Turbulence intensity of the wall shear stress.

Q_F and Q_S is equal to the energy added to the hot-film, thus regarded as the output signal of the sensor, when it is operated at the constant temperature.

RESULTS

Temperature distribution

The computed mean temperature distribution is shown in Fig. 3, comparing the result for two different wall materials, acrylic and aluminum. The coordinates are normalized by the sensor span. It is clear that the temperature distribution on the surface exposed to the fluid flow is strongly influenced by the wall material, namely, the thermal conductivity of the wall. Because of the large heat conduction into the aluminum wall, cf. (c) and (d), the heat conduction along the wall surface is relatively small as compared to that resulted from the computation for the acrylic wall, resulting in the enlargement of the effective sensor size, cf. (a) and (b). Moen and Schneider (1993) have reported the similar result obtained from their measurement.

The heat conducted in the substrate is the consequence of the low thermal conductivity of the wall material relative to that of the substrate. The performance of the hot-film sensor is considered to be strongly influenced by this relationship. Therefore, the insulation of the

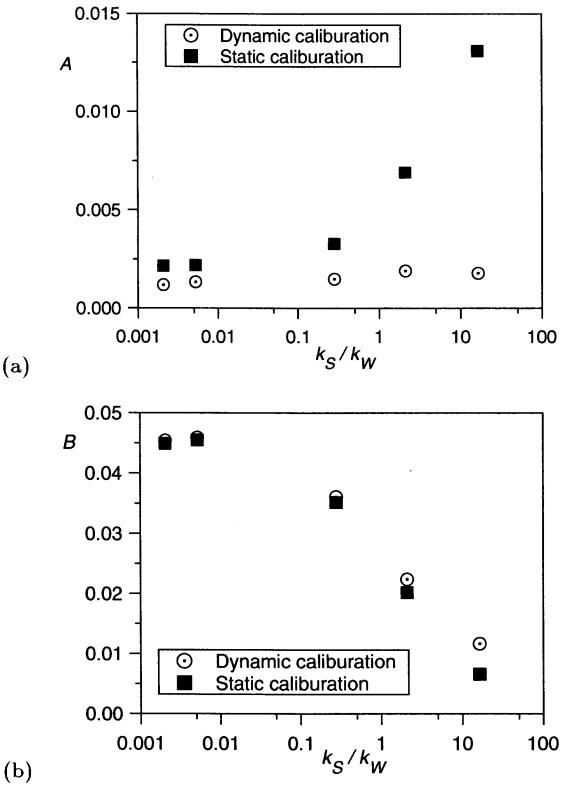

Figure 5: Coefficients determined by dynamic calibration.

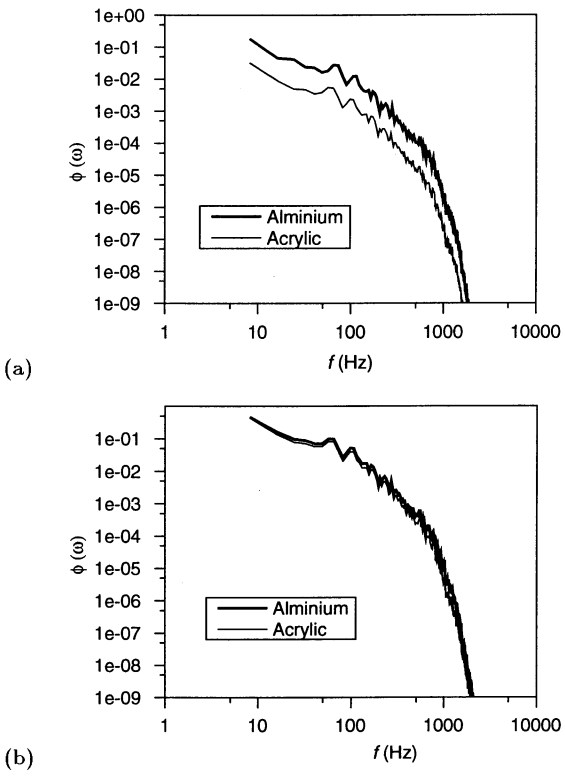

Figure 6: Spectrum of the fluctuating wall shear stress, (a) static calibration, (b) dynamic cariblation.

hot-film from the wall leads to the undesired situation as long as the substrate exists.

Effect of dynamic calibration

The turbulence statistics of the wall shear stress, calculated by Eq. (1), is summarized in Table 2 for various wall materials. The "true" value obtained by the present DNS is shown at the bottom of the table. The turbulence intensity of wall shear stress, τ_w', is obviously underestimated by the hot-film, which is common in experiments. The largest value is provided by the wall made of aluminum, which has the largest thermal conductivity among all, while the case of cavity made below substrate is the worst. The comparison with the other studies are also shown in Fig. 4. The horizontal axis is scaled by the ratio of thermal conductivity of the substrate and that of wall material. The right most plot of the present study corresponds to the case of cavity.

The dependency of τ_w' on the wall material is the consequence of the statistic calibration by which the empirical constants A and B are determined. Clearly, the calibration undertaken at the steady condition is not applicable to the fluctuating flow. In the present case, where the true value is known, it is possible to calibrate these coefficients so as to obtain the desired value of τ_w'. Figures 5 shows the

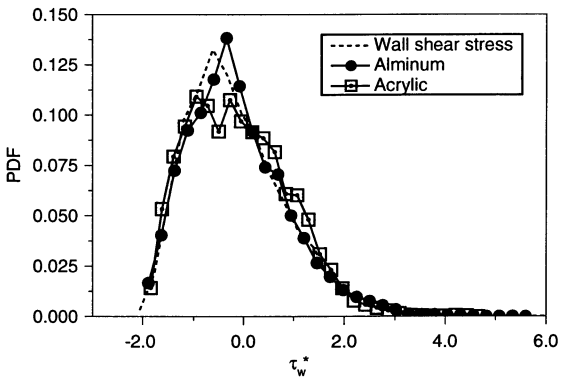

Figure 7: Probability density function of the wall shear stress.

consequence of such attempt. The necessary correction for constant A is much larger than for B. It is interesting that A stays nearly constant for various wall materials, while B is a strong function of the thermal conductivity ratio. This fact suggests that the heat loss due to the conduction appears in the pedestal level of the signal, but the frequency characteristics stay almost unchanged.

The effect of the dynamic calibration is further examined in Fig. 6, where the spectra of fluctuating wall shear stress is compared for two typical wall materials, aluminum and acrylic. When the wall shear stress signal is calibrated in the conventional manner, as shown in (a) for static case, the difference in the wall material is obvious for the entire fre-

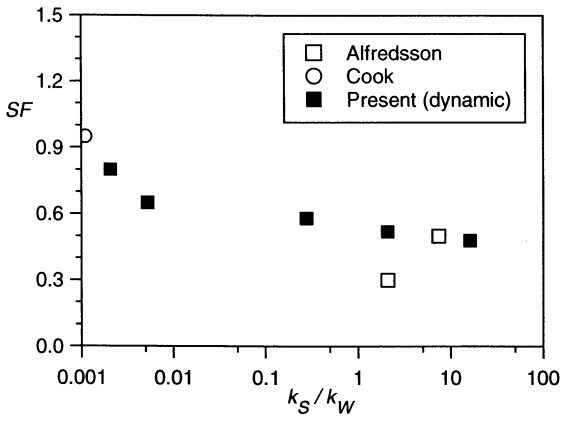

Figure 8: Skewness factor of the wall shear stress.

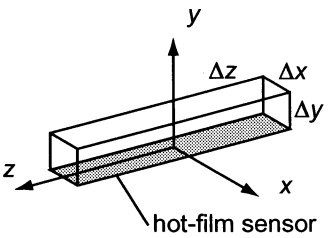

Figure 9: Control volume for the evaluation of convective heat flux above the hot-film.

quency range. However, when the dynamic calibration is applied, the two curves overlap and almost indistinguishable from each other. It is therefore concluded that the heat loss by the conduction into the wall does not contribute to alter the frequency characteristics of the hot-film output.

Higher-order moment

The practice of dynamic calibration described above suggests that the heat loss due to conduction to the wall is not a major cause for the contamination of hot-film output. However, it does not necessarily mean that the difference in heat conduction does not alter the turbulence statistics. It is now demonstrated that the higher-order statistics, i.e., skewness factor, is indeed influenced. The probability density function obtained from the acrylic wall and aluminum, both after the dynamic calibration, are compared in Fig 7. The horizontal axis shows the normalized wall shear stress, $\tau_w^* \equiv (\tau_w - \overline{\tau}_w)/\tau_w'$. As summarized in Table 2, the skewness factor (SF) after the dynamic calibration is 0.52 for the acrylic wall, while the aluminum wall provides SF=0.80. The difference is also seen in the distribution of PDF.

DISCUSSION

The cause for the difference found in the skewness factor is further investigated in connection with the thermal transport around to the sensor. The instantaneous convective heat flux q_x', q_y' and q_z' are defined by:

$$q_x' = \iiint \frac{\Delta(u'T')}{\Delta x} dx\, dy\, dz, \quad (5)$$

$$q_y' = \iiint \frac{\Delta(v'T')}{\Delta y} dx\, dy\, dz, \quad (6)$$

$$q_z' = \iiint \frac{\Delta(w'T')}{\Delta z} dx\, dy\, dz, \quad (7)$$

where T' denotes the fluctuating component of temperature. The volume integration is evaluated for the control volume as shown in Fig. 9, and the difference is calculated for each direction. The variation of these quantities is directly related to the output of the hot-film sensor.

Figure 10 shows the temporal variation of the convective heat flux around the sensor. The graph on the left is for the acrylic wall, while the right one corresponds to the case for aluminum wall. Not that the time $t = 0$ does not correspond to the initial condition of simulation, but to a certain instant when the variation of q' indicate a characteristic signal: The two graphs are taken from the same record of fluid flow DNS. It is remarkable that the signal of the computation with aluminum wall shows the fluctuation with larger amplitude and more rapid variation for $0 \leq t \leq 0.005$s. The difference in the skewness factor due to the wall material is explained by this comparison.

Figure 11 shows the same instant as marked in Fig. 10. It is indicated that the rapid variation found in the signal in aluminum wall computation corresponds to the instant at which a streaky structure passed over the sensor. The signal output from the acrylic wall has completely missed the rapid variation. It is clear that the rapid and intermittent variation of q_x' is only possible when the streamwise gradient of $u'T'$ is captured correctly. When the temperature distribution around the sensor is considered, cf. Fig. 3, the hot-film sensor attached on the acrylic wall is elongated in the streamwise direction, and therefore the streamwise temperature gradient cannot be captured at any instant.

In summary, the influence of the heat conduction to the wall is determined by the thermal conductivity, but the frequency characteristics has rather minor effect. The material of low thermal conductivity behind the substrate hinder the heat release into the wall and causes the streamwise elongation of the sensor. When

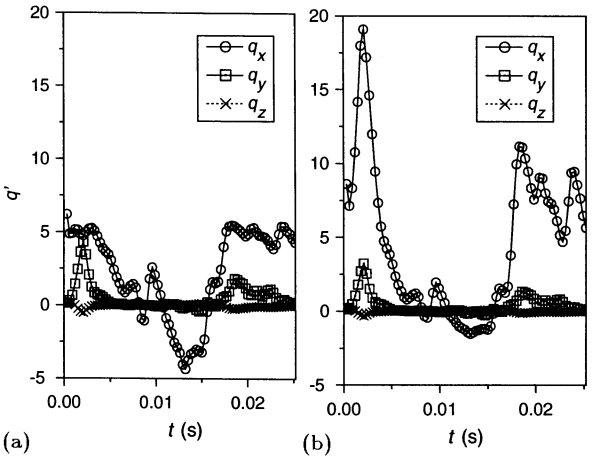

Figure 10: Evolution of the convective heat flux from the hot-film sensor. (a) Acrylic wall, (b) alminum wall.

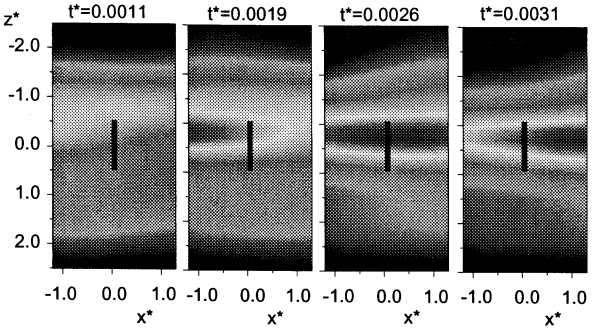

Figure 11: Streaky structure passing over the hot-film sensor.

a rapid response is desired, it is recommended that the substrate has sufficiently lower thermal conductivity than the material of the wall to which the hot-film sensor is adhered.

CONCLUDING REMARKS

The influence of the heat conduction into the wall on the hot-film signal has been numerically investigated. It is shown that the static calibration of the hot-film provides too low a turbulence intensity. The dynamic calibration is possible by refereeing to the thermal conductivity of the wall material and the substrate of the hot-film. However, the rapid and intermittent variation of the wall shear stress is only captured by the sensor that has sufficient streamwise resolution realized by the appropriate heat release to the wall.

ACKNOWLEDGEMENT

The authors are grateful to Prof. T. Kajishima of Osaka University, Japan, for providing the basic code for DNS computation.

REFERENCES

Alfredsson, P. H., Johansson, A. V., Haritonidis, J. H. and Eckelmann, H. 1988 The Fluctuating Wall-Shear Stress and the Velocity Field in the Viscous Sublayer. *Phys. Fluids* **31**, 1026–1033.

Chambers, F. W., Murphy, H. D. and McEigot, D. M. 1982 Laterally Converging Flow Part2: Temporal Wall Shear Stress. *J. Fluid Mech.* **127**, 403–428.

Cook, W. J. 1994 Response of Hot-Wlement Wall Shear Stress Gages in Unsteady Turbulent Flow, *AIAA J.* **32**, 1464–1471.

Dengel, P., Fernholz, H. H. and Hess, M. 1987 Skin-Friction Measurements in Two- and Three-Dimensional Highly Turbulent Flows with Separation. in *Advances in turbulence 1*, Springer, 470–479.

Eckelmann, H. 1974 The Structure of the Viscous Sublayer and the Adjacent Wall Region in a Turbulent Channel Flow. *J. Fluid Mech.* **65**, 439–459.

Kajishima, T., Ohta, T., Okazaki, K., Miyake,Y. 1998 High-Order Finite-Difference Method for Incompressible Flows using Collocated Grid System. *JSME Int. J., Ser. B*, **41**, 830–839.

Kimura, M., Tung, S., Lew, J., Ho, C. M., Jiang, F. and Tai, Y. C. 1999 Measurements of Wall Shear Stress of a Turbulent Boundary Layer Using a Micro-Shear-Sterss Imaging Chip. *Fluid Dynamic Research* **24**, 329–342.

Kim, J., Moin, P. and Moser, R. 1987 Turbulent Statics in Fully Developed Channel Flow at Low Reynolds Number. *J. Fluid Mech.* **177**, 133–160.

Moen, M. J. and Schneider, S. P. 1993 The Effect of Sensor Size and Substrate Properties on the Performance of Flush-Mounted Hot-Film Sensors, *ASME-FED Vol.167, Thermal Anemometry*, 249–261.

Moen, M. J. and Schneider, S. P. 1994 The Effect of Sensor Size on the Performance of Flush-Mounted Hot-Film Sensors, *Trans. ASME, J. Fluids Engineering*, **116**, 273–277.

Obi, S., Inoue, K., Frukawa, T. and Masuda, S. 1996 Experimental Study on the Statistics of Wall Shear Stress in Turbulent Channel Flows. *Int. J. Heat Fluid Flow*, **17**, 187–192.

Reda, D. C. 1991 Rise-Time Response of Nickel-Foil-on-Kapton-Substrate, Hot-Film, Shear-Stress Sensors. *AIAA Paper 91-0169.*

Tardu, S., Pham, C. T. and Binder, G. 1991 Effects of longitudinal difusion in the fluid and of heat conduction to the substrate on the response of wall hot-film gages. in *Advances in Turbulence* 3, A. V. Johansson and P. H. Alfredsson (eds.), Springer-Verlag.